An Acad Bras Cienc (2024) 96(2): e20230953 DOI 10.1590/0001-3765202420230953
Anais da Academia Brasileira de Ciências | *Annals of the Brazilian Academy of Sciences*
Printed ISSN 0001-3765 I Online ISSN 1678-2690
www.scielo.br/aabc | www.fb.com/aabcjournal

ENGINEERING SCIENCES

Response Surface Model of the Reduced Flexibility Matrix for Bayesian Damage Identification

LEONARDO T. STUTZ, DIEGO C. KNUPP, LUIZ ALBERTO S. ABREU, ISABELA CRISTINA S.S. RANGEL, LUCIANO S. RANGEL & ROSILENE A.P. CORRÊA

Abstract: The present work is concerned with the use of a Response Surface Model of the reduced flexibility matrix for structural damage identification. A Response Surface Model (RSM) is fitted with the aim at providing a polynomial relationship between nodal cohesion parameters, used to describe the damage field within the structure, and elements of the reduced flexibility matrix. A design of experiment built on combinations of a relatively small number of nodal cohesion parameters is used to fit the RSM. The damage identification problem is formulated within the Bayesian framework and the Delayed Rejection Adaptive Metropolis method is used to sample the posterior probability density function of the uncertain cohesion parameters. Numerical simulations addressing damage identification in plates were carried out in order to assess the proposed approach, which succeeded in the identification of the different damage profiles considered. Besides, the use of a RSM, instead of a FEM of the structure, resulted in reductions of up almost 78**%** in the required computational cost.

Key words: Adaptive metropolis, bayesian inference, damage identification, delayed rejection, reduced flexibility matrix, response surface model.

INTRODUCTION

Damage identification (DI) approaches are of prime importance for maintaining the functionality and even the integrity of engineering structures. In the last decades, vibration-based DI approaches have received considerable attention from the scientific and engineering communities. Differently from classical non-destructive testing, such as X-ray and ultrasound (Rens et al. 1997), vibration-based DI approaches are based on global dynamic characteristics of the structure being evaluated, thus not requiring a prior knowledge of the damage location nor that this portion of the structure is readily accessible for inspection (Hou & Xia 2021, Ereiz et al. 2022, Randall 2021, Kong et al. 2017).

Vibration-based DI approaches are built on the premise that the presence of structural damages alters the dynamic behavior of the structure, which in turn can be quantified through vibration measurements and used to infer about its integrity. Damage identification problems are usually posed as inverse problems of parameter estimation, where a set of parameters of a model of the structure is estimated in order to ensure that predictions of the updated model resemble corresponding observed

experimental data, as closely as possible (Hou & Xia 2021, Ereiz et al. 2022, Randall 2021, Kong et al. 2017).

Inverse problems of parameter estimation are typically ill-posed and ill-conditioned, due to the limited information in the observed experimental data and the presence of measurement noise, parameter uncertainties and model discrepancy (also known as inadequacy or bias) (Kirsch 1996, Gardner et al. 2021). A robust probabilistic approach for the formulation of inverse problems of parameter estimation, in special the damage identification problems, to handle measurement errors and parameter and modelling uncertainties are provided by the Bayesian framework (Kong et al. 2017, Kaipio & Somersalo 2004, Beck & Au 2002, Yuen & Kuok 2011). In the Bayesian statistical framework, the uncertain parameters of the model are treated as random variables and the objective is to infer about their joint posterior probability density function conditioned on observed experimental data. The joint posterior probability density function describes all plausible values for the uncertain model parameters based on the available experimental data. Further, the Bayesian framework also provides robust probabilistic approaches for model class selection and model averaging. In the Bayesian model class selection, given a set of probabilistic model classes, the plausibility of each probabilistic model class to describe the system behaviour, based on measured data, is computed. Then, the most plausible model class based on the available measured data is accessed. In cases where there are more than one plausible model class, with the Bayesian model averaging, the expected value of any quantity of interest, conditioned on the measured data and all the competing model classes, may be computed (Beck & Au 2002, Yuen & Kuok 2011, Marwala et al. 2016, Huang et al. 2018, Ching & Chen 2007).

In practical Bayesian inference problems, the joint posterior probability density function of the uncertain parameters is usually estimated by numerical sampling methods, such as the Markov Chain Monte Carlo (MCMC) methods. In these methods, samples are drawn from an auxiliary density function with the aim at generating an ergodic Markov chain whose stationary distribution is the desired one. Due to its simplicity, the Metropolis-Hastings (MH) algorithm is one of the most used MCMC methods (Kaipio & Somersalo 2004). However, the MH algorithm may become inefficient when sampling multimodal posterior probability density functions, when the uncertain parameters are highly correlated, or when they are defined in a highly dimensional space (Beck & Au 2002, Ching & Chen 2007, Gamerman & Lopes 2006). In such cases, an extremely large number of samples along with a long burn-in period may be required to sample the desired probability density function. Even so, a poor sampling can be obtained. Therefore, with the aim at improving the sampling capabilities and/or the computational efficiency of conventional sampling methods, several advanced MCMC methods has been proposed, such as Hamiltonian Monte Carlo methods (Neal 2011, Cheung & Beck 2009), Multiple Try MCMC methods (Martino 2018, Martino & Read 2013), the Delayed Rejection Adaptive Metropolis method (Haario et al. 2006), the Transitional Markov Chain Monte Carlo method (Ching & Chen 2007, Ching & Wang 2016), and Sequential Monte Carlo Methods (Liu & Chen 1998, Dessi & Camerlengo 2015), to cite a few.

The use of finite element models (FEMs) in damage identification approaches is popular, because they provide information about damage location and damage extent. In some cases, they can also allow for response prediction and damage prognosis (Prakash & Narasimhan 2018, Kong et al. 2017). However, since the numerical sampling of the posterior probability density function of the uncertain

parameters requires the computation of the model response at each sample drawn, the use of a FEM of the structure may yield an extremely high computational cost. Hence, in order to obtain a computationally more efficient damage identification approach, the FEM of the structure may be replaced by a surrogate model. Different surrogate models have been successfully applied in damage identification problems, such as Artificial Neural Networks (Sbarufatti et al. 2013, Rocchetta et al. 2018, Lye et al. 2021), Kriging surrogate models (Jin & Jung 2016, Ghiasi et al. 2018), Gaussian Process Regression (Ramancha et al. 2022, Talaei et al. 2018, Ni et al. 2021) and Response Surface Models (Stutz et al. 2018, Fang & Perera 2011, Umar et al. 2018).

The present work addresses the structural damage identification problem in plates, which are important structural components in automotive, aeronautical, civil and naval engineering (Huang & Schröder 2021, Fu et al. 2013, Simoen et al. 2015, Silva et al. 2020, 2021, Li et al. 2022, Chen et al. 2018). The proposed damage identification approach is formulated within the Bayesian framework and it is built on a RSM (Myers et al. 2009) of the reduced flexibility matrix of the structure. Here, the damage state of the structure is described by a set of cohesion parameters and the RSM provides a polynomial relationship between these parameters and elements of the reduced flexibility matrix of the structure, yielding a computationally more efficient damage identification approach. The Delayed Rejection Adaptive Metropolis (DRAM) (Haario et al. 2006) is used to sample the joint posterior probability density function of the uncertain parameters. Basically, the DRAM combines two strategies: the Adaptive Metropolis (AM) (Haario et al. 2001) and the Delayed Rejection (DR) (Mira 2001). The adaptive strategy of the method allows the tuning of the auxiliary density function based on past samples in order to better reflect the target probability distribution, whereas the delayed rejection allows multiple stages of proposal samples at each iteration, which can help explore multimodal distributions more effectively (Warner et al. 2016).

The proposed approach is numerically assessed considering damage identification problems in a simply supported Kirchhoff plate. Three different damage scenarios and three different noise levels corrupting the synthetic experimental mode shapes of the structure are addressed. The numerical results show that the adopted strategy for training the RSM of the structure requires a considerably small number of numerical simulations in order to provide the corresponding training data, increasing, therefore, the applicability of RSM-based damage identification approaches. Besides, the numerical results also show that the proposed damage identification approach succeeded in providing accurate information about the existence, location and extent of structural damages in all addressed cases.

MATHEMATICAL MODELLING

This section is devoted to present the basic concepts related to the synthesis of a Response Surface Model of the reduced flexibility matrix of a damaged plate, whose integrity is continuously described by a cohesion field.

Damage model

It is assumed that the stiffness properties of a supposedly damaged structure may be used to assess its structural integrity (Randall 2021, Kong et al. 2017). In addition, it is also assumed that the dynamic

tests required for damage identification do not suffice to alter the structural integrity of the tested structure.

The flexural stiffness of a plate, at a point (x, y) within its middle surface in undeformed position, is defined as

$$D(x,y) = \frac{E(x,y)h(x,y)^3}{12\,[1 - \nu(x,y)^2]}, \tag{1}$$

where E is the Young's modulus, h is the thickness of the plate, ν is the Poisson's ratio (Leissa & Qatu 2011).

Aiming at describing the damage as a stiffness loss in the structure, the flexural stiffness may be rewritten as

$$D(x,y) = \beta(x,y)D_0, \tag{2}$$

where the cohesion filed $\beta(x,y)$ is the function used to describe the damage within the structure, and D_0 is the nominal flexural stiffness of the undamaged plate, given by

$$D_0 = \frac{E_0 h_0^3}{12\left(1 - \nu_0^2\right)}, \tag{3}$$

where E_0 is the nominal Young's modulus, h_0 is the nominal thickness of the plate, ν_0 is the nominal Poisson's ratio.

Considering Eq. (2), the elemental stiffness matrix of a rectangular finite element of a Kirchhoff plate may be written as

$$\mathbf{K}^e = \int_{\Omega_e} \beta^e(\bar{x},\bar{y}) \frac{E_0 h_0^3}{12\left(1 - \nu_0^2\right)} \mathbf{B}^T \bar{\mathbf{D}} \mathbf{B}\, d\bar{x} d\bar{y}, \tag{4}$$

where $\beta^e(\bar{x},\bar{y})$ stands for the cohesion field within the finite element, $\bar{x}$ and $\bar{y}$ are in-plane local coordinates, Ω_e stands for the elastic domain of the element and the matrices $\bar{\mathbf{D}}$ and $\mathbf{B}$ are, respectively, given by

$$\bar{\mathbf{D}} = \begin{bmatrix} 1 & \nu & 0 \\ \nu & 1 & 0 \\ 0 & 0 & \frac{1-\nu}{2} \end{bmatrix}, \tag{5}$$

$$\mathbf{B} = \begin{bmatrix} \frac{\partial^2 N_1(\bar{x},\bar{y})}{\partial \bar{x}^2} & \frac{\partial^2 N_2(\bar{x},\bar{y})}{\partial \bar{x}^2} & \cdots & \frac{\partial^2 N_{12}(\bar{x},\bar{y})}{\partial \bar{x}^2} \\ \frac{\partial^2 N_1(\bar{x},\bar{y})}{\partial \bar{y}^2} & \frac{\partial^2 N_2(\bar{x},\bar{y})}{\partial \bar{y}^2} & \cdots & \frac{\partial^2 N_{12}(\bar{x},\bar{y})}{\partial \bar{y}^2} \\ \frac{\partial^2 N_1(\bar{x},\bar{y})}{\partial \bar{x}\partial \bar{y}} & \frac{\partial^2 N_2(\bar{x},\bar{y})}{\partial \bar{x}\partial \bar{y}} & \cdots & \frac{\partial^2 N_{12}(\bar{x},\bar{y})}{\partial \bar{x}\partial \bar{y}} \end{bmatrix}, \tag{6}$$

where N_i, $i = 1, \ldots, 12$ are appropriate interpolation functions (Reddy 1984).

In the present work, the same finite element mesh was used to spatially discretize both the displacement and the cohesion fields. Besides, within a finite element, the cohesion field was interpolated as

$$\beta^e(\bar{x},\bar{y}) \approx R_1^e(\bar{x},\bar{y})\beta_1^e + R_2^e(\bar{x},\bar{y})\beta_2^e + R_3^e(\bar{x},\bar{y})\beta_3^e + R_4^e(\bar{x},\bar{y})\beta_4^e, \tag{7}$$

where $R_i^e(\bar{x}, \bar{y})$ and β_i^e, $i = 1, \ldots, 4$, are, respectively, bilinear shape functions and nodal cohesion parameters, that is, values of the cohesion field at the corner nodes of the finite element.

Considering the spatial discretization of the cohesion field, the damage state of the structure is, therefore, described by the vector of nodal cohesion parameters

$$\boldsymbol{\beta} = \begin{bmatrix} \beta_1 & \beta_2 & \ldots & \beta_{n_p} \end{bmatrix}^T, \tag{8}$$

where β_i represents the value of the cohesion parameter at the *i-th* global node of the spatial discretization of this field and n_p is the total number of nodes.

Flexibility matrix

The flexibility matrix of a structure is defined as the inverse of the stiffness matrix and it can be written in terms of the modal parameters as

$$\mathbf{G} = \boldsymbol{\Phi}\boldsymbol{\Lambda}^{-1}\boldsymbol{\Phi}^T = \sum_{i=1}^{n} \frac{1}{\omega_i^2} \boldsymbol{\phi}_i \boldsymbol{\phi}_i^T, \tag{9}$$

where $\boldsymbol{\Lambda} = \text{diag}[\omega_1^2, \omega_2^2, \ldots, \omega_n^2]$ is a diagonal matrix containing the squared undamped natural frequencies of the structure, n is the number of degrees of freedom (DOFs), $\boldsymbol{\Phi} = \begin{bmatrix} \boldsymbol{\phi}_1 & \boldsymbol{\phi}_2 & \ldots & \boldsymbol{\phi}_n \end{bmatrix}$ is the corresponding modal matrix, whose columns are the mass-normalized undamped mode shapes and T stands for the matrix transpose operator.

The undamped modal parameters of the structure may be obtained from the generalized eigenvalue problem

$$(\mathbf{K} - \omega_i^2 \mathbf{M})\boldsymbol{\phi}_i = \mathbf{0}, \qquad i = 1, 2, \ldots, n, \tag{10}$$

where $\mathbf{M}$ and $\mathbf{K}$ are, respectively, the $n \times n$ mass and stiffness matrices of the finite element model of the structure (FEM) (Meirovitch 1986). Besides, for mass-normalized mode shapes, one has

$$\begin{aligned} \boldsymbol{\Phi}^T \mathbf{M} \boldsymbol{\Phi} &= \mathbf{I}; \\ \boldsymbol{\Phi}^T \mathbf{K} \boldsymbol{\Phi} &= \boldsymbol{\Lambda}. \end{aligned} \tag{11}$$

Due to practical limitations inherent to modal tests, as the limited number of measured DOFs and the limited number of excited modes of vibration, the following approximation for the flexibility matrix may be experimentally obtained

$$\mathbf{G}_E = \sum_{i=1}^{n_E} \frac{1}{\omega_{iE}^2} \boldsymbol{\phi}_{iE} \boldsymbol{\phi}_{iE}^T, \tag{12}$$

where $n_E < n$ is the number of modes obtained from the modal test, ω_{iE} and $\boldsymbol{\phi}_{iE}$ are, respectively, the i-th undamped natural frequency and corresponding undamped mode shape experimentally obtained (Alvin et al. 2003).

It must be emphasized that if only m DOFs of the structure are measured in the modal test, the experimental mode shapes $\boldsymbol{\phi}_{iE}$, $i = 1, \ldots, n_E$, are vectors with dimension $m \times 1$. Therefore, according to Eq. (12), despite the number n_E of obtained modes, the experimentally derived flexibility matrix $\mathbf{G}_E$

has order m. Since the structural flexibility matrix $\mathbf{G}$, defined in Eq. (9), has order n, for the formulation of the damage identification problem, the following reduced order flexibility matrix is required.

$$\bar{\mathbf{G}} = \sum_{i=1}^{n_E} \frac{1}{\omega_i^2} \bar{\boldsymbol{\phi}}_i \bar{\boldsymbol{\phi}}_i^T, \tag{13}$$

where $\bar{\boldsymbol{\phi}}_i$ represents the i-th mode shape of the structure, provided by the FEM, and whose components are only the m DOFs related with the corresponding ones measured in the modal test.

Response Surface Model of the flexibility matrix

With the aim at obtaining a computationally more efficient approach for solving the damage identification problem, the reduced flexibility matrix of the FEM of the structure, given by Eq. (13), is replaced by a corresponding Response Surface Model (RSM) in the formulation of the inverse problem. Therefore, a RSM is defined here so as to provide explicit relations between nodal cohesion parameters of the structure and elements of the reduced flexibility matrix. The synthesis of the RSM is presented next and it is in accordance with the one presented in (Stutz et al. 2018).

Given an element $\bar{G}_{ij}$ of the reduced flexibility matrix, one defines

$$\bar{G}_{ij} = f(\bar{\beta}_1, \bar{\beta}_2, \dots, \bar{\beta}_{n_p}) + \varepsilon, \tag{14}$$

where f is a response surface, ε represents the error in the model prediction, and $\bar{\beta}_i \in [-1, 1]$ are coded nodal cohesion parameters, which are defined as

$$\bar{\beta}_i = \frac{\beta_i - 0.5\left(\beta_{\text{low}} + \beta_{\text{high}}\right)}{0.5\left(\beta_{\text{high}} - \beta_{\text{low}}\right)}, \qquad i = 1, 2, \dots, n_p, \tag{15}$$

where β_{low} and β_{high} are, respectively, the low and high values of the cohesion parameters considered in the definition of the Response Surface Model.

The following response surface, given by a second order polynomial accounting for interaction effects between two arbitrary coded parameters, is adopted.

$$f(\bar{\beta}_1, \bar{\beta}_2, \dots, \bar{\beta}_{n_p}) = \alpha_0 + \sum_{i=1}^{n_p} \alpha_i \bar{\beta}_i + \sum_{i=1}^{n_p} \alpha_{ii} \bar{\beta}_i^2 + \sum_{i<j} \sum_{j=2}^{n_p} \alpha_{ij} \bar{\beta}_i \bar{\beta}_j, \tag{16}$$

where α_i, α_{ii} e α_{ij} are the coefficients of the adopted response surface, which are determined as follows.

For a specific damage scenario, described by the vector of cohesion parameters $\boldsymbol{\beta}$, one may compute the elements of the reduced flexibility matrix $\bar{G}_{ij}$, provided by the FEM of the structure, and the corresponding coded parameters $\bar{\beta}_i$, $i = 1, \dots, n_p$, according to Eqs. (13) and (15), respectively. Therefore, for a given element of the reduced flexibility matrix, one has a training datum given by $(\bar{\beta}_1, \dots, \bar{\beta}_{n_p}; \bar{G}_{ij})$ for the synthesis of the response surface. Hence, considering a set of n_d training data, obtained from n_d different damage scenarios, one has

$$\mathbf{g} = \mathbf{X}\boldsymbol{\alpha} + \boldsymbol{\varepsilon}, \tag{17}$$

where $\mathbf{g}$ is the vector composed with the n_d values of the considered element $\bar{G}_{ij}$ of the reduced flexibility matrix, $\mathbf{X}$ is the project matrix, whose elements are obtained from the coded parameters $\bar{\beta}_i$, $\boldsymbol{\alpha}$ is the vector with the coefficients of the response surface given by Eq. (16), and $\boldsymbol{\varepsilon}$ is the vector with the corresponding errors in the model predictions.

According to Eq. (16), the number of coefficients of the adopted response surface is given by $n_c = (n_p + 1)(n_p + 2)/2$. Therefore, one must have a number of training data n_d greater than or equal to n_c for a proper estimation of the response surface coefficients. Considering Eq. (17), an unbiased estimate for the vector of coefficients $\boldsymbol{\alpha}$ is given by (Myers et al. 2009)

$$\hat{\boldsymbol{\alpha}} = \left(\mathbf{X}^T\mathbf{X}\right)^{-1}\mathbf{X}^T\mathbf{g}. \tag{18}$$

Therefore, the RSM of the element $\bar{G}_{ij}$ of the reduced flexibility matrix is given by

$$\hat{\bar{G}}_{ij} = \hat{\alpha}_0 + \sum_{i=1}^{n_p}\hat{\alpha}_i\bar{\beta}_i + \sum_{i=1}^{n_p}\hat{\alpha}_{ii}\bar{\beta}_i^2 + \sum_{i<j}\sum_{j=2}^{n_p}\hat{\alpha}_{ij}\bar{\beta}_i\bar{\beta}_j. \tag{19}$$

Aiming at the formulation of the damage identification problem, the generalized response vector, comprised of elements of the reduced flexibility matrix provided by the RSM, is defined as

$$\hat{\boldsymbol{z}} = \left[\hat{\bar{G}}_{11} \quad \hat{\bar{G}}_{12} \ldots \hat{\bar{G}}_{1m} \quad \hat{\bar{G}}_{22} \quad \hat{\bar{G}}_{23} \ldots \hat{\bar{G}}_{2m} \ldots \hat{\bar{G}}_{mm}\right]^T, \tag{20}$$

where m is the number of columns (or lines) of the reduced flexibility matrix. One should note that, due to the symmetry of the reduced flexibility matrix, not all of its components are considered in the definition of the generalized response vector $\hat{\boldsymbol{z}}$ in Eq. (20).

Training data of the RMS

Fitting a Response Surface Model requires an appropriate choice of training data. As aforementioned, in the present case, for fitting a RSM of a given element of the reduced flexibility matrix, one requires n_d training data, where one training datum is given by $(\bar{\beta}_1, \ldots, \bar{\beta}_{n_p}; \bar{G}_{ij})$, where $\bar{\beta}_i$, $i = 1, \ldots, n_p$, are the coded values of the components of a prescribed vector of cohesion parameters, which describes a specific damage scenario, and $\bar{G}_{ij}$ is the corresponding element of the reduced flexibility matrix provided by the FEM of the structure. Once the training data are obtained, the coefficients of the RSM of an element of the reduced flexibility matrix are computed according to Eq. (18).

Different design of experiments are presented in the specialized literature with the aim at designing experiments (or numerical simulations) to provide meaningful training data for the synthesis of RSMs and other surrogate models. Among them, the Center Composite Design (CCD) is the most popular design of experiment used to fit second-order polynomial response surface models (Myers et al. 2009). However, depending on the number of model parameters (the nodal cohesion parameters, in the present case), the CCD may require a prohibitively great number of experimental tests (or numerical simulation runs) in order to provide the desired training data. For instance, considering a model with n_p parameters, the number of training data required for a CCD is given by 2^{n_p} factorial points, added with $2n_p$ axial points and n_0 central points (Montgomery 2006).

The training data of the RSM are chosen based on the following practical assumptions: 1. The damage identification approach is capable of identifying structural damages in an early stage; 2. The

structural damages are localized events, which means that damaged regions occupy relatively small portions of the structure domain. Therefore, the damage state is supposed to be described by a relatively very small number of nodal cohesion parameters that will take values different from unity. Hence, the training data of the RSM may be obtained based on Combinations of a relatively small number of cohesion parameters (Montgomery & Runger 2014), which will require a considerably lower number of experimental tests (or numerical simulations) in order to generate the corresponding data, when compared with the CCD method.

DAMAGE IDENTIFICATION PROBLEM

Formulation of the Bayesian damage identification problem

In the present work, the inverse problem of damage identification is posed as a Bayesian inference problem. Therefore, the vector of unknown parameters $\boldsymbol{\theta}$, which is composed of the total or a subset of the nodal cohesion parameters of the structure, is assumed as a random variable and the main objective is to determine the posterior joint probability density function (PDF) of these unknown parameters.

According to Bayes theorem, the joint posterior PDF of the unknown parameters is given by

$$p(\boldsymbol{\theta}|\mathbf{z}_E) = \frac{p(\mathbf{z}_E|\boldsymbol{\theta})p(\boldsymbol{\theta})}{p(\mathbf{z}_E)} \tag{21}$$

where $\mathbf{z}_E$ is the generalized experimental response vector, whose components are elements of the experimental flexibility matrix, given by Eq. (12), $p(\mathbf{z}_E|\boldsymbol{\theta})$ is the likelihood function, $p(\boldsymbol{\theta})$ is the prior probability density function, which describes the information one has about the parameters before considering any information about the experimental data, and $p(\mathbf{z}_E)$ represents the distribution of the experimental data,

$$p(\mathbf{z}_E) = \int_{\Theta} p(\mathbf{z}_E|\boldsymbol{\theta})p(\boldsymbol{\theta})d\boldsymbol{\theta}, \tag{22}$$

which acts as a normalizing constant in a parameter estimation problem of a given model (Kaipio & Somersalo 2004).

The observation model is assumed as

$$\mathbf{z}_E = \hat{\mathbf{z}}(\boldsymbol{\theta}) + \boldsymbol{\epsilon}, \tag{23}$$

where $\boldsymbol{\epsilon}$ is a vector accounting for measurement errors. Therefore, according to the adopted observation model, the experimental response $\mathbf{z}_E$ is supposed to be explained by the model prediction $\hat{\mathbf{z}}(\boldsymbol{\theta})$ and the measurement error vector $\boldsymbol{\epsilon}$.

Assuming that the measurement error $\boldsymbol{\epsilon}$ is independent of the unknown parameter $\boldsymbol{\theta}$ and that it is normally distributed, with zero mean and a covariance matrix $\mathbf{W}$, the likelihood function is given by

$$p(\mathbf{z}_E|\boldsymbol{\theta}) = \frac{1}{\sqrt{(2\pi)^{n_z}\det(\mathbf{W})}} \exp\left[-\frac{1}{2}\left(\mathbf{z}_E - \hat{\mathbf{z}}(\boldsymbol{\theta})\right)^T \mathbf{W}^{-1}\left(\mathbf{z}_E - \hat{\mathbf{z}}(\boldsymbol{\theta})\right)\right], \tag{24}$$

where n_z is the number of components in the response vectors $\mathbf{z}_E$ and $\hat{\mathbf{z}}(\boldsymbol{\theta})$.

In the present work, a Markov Chain Monte Carlo (MCMC) method was used to infer about the joint posterior PDF of the unknown parameters $p(\boldsymbol{\theta}|\mathbf{z}_E)$ (Kaipio & Somersalo 2004). Samples of the target PDF were drawn by the Delayed Rejection Adaptive Metropolis algorithm.

Delayed Rejection Adaptive Metropolis

The Delayed Rejection Adaptive Metropolis (DRAM) algorithm, proposed by Haario et al. (2006), basically combines two strategies: the Adaptive Metropolis (AM) (Haario et al. 2001) and the Delayed Rejection (DR) (Mira 2001). The algorithm is briefly described in what follows.

Given a current state $\boldsymbol{\theta}_n$ of the Markov Chain, the auxiliary probability density function of the first stage of the DR algorithm is a multivariate Gaussian, centred at the current state and with covariance matrix $\mathbf{C}_n^1$ given by the AM strategy

$$\mathbf{C}_n^1 = \begin{cases} \mathbf{C}_0, & n \leq n_0 \\ s_d \text{Cov}(\boldsymbol{\theta}_0, \boldsymbol{\theta}_1, ..., \boldsymbol{\theta}_{n-1}) + s_d \lambda \mathbf{I}_d, & n > n_0 \end{cases} \tag{25}$$

where n_0 is the length of the initial non-adaptation period, $\mathbf{C}_0$ is an arbitrary strictly positive definite matrix, representing the covariance matrix of the auxiliary density during the non-adaptation period, s_d is a parameter that depends only on the dimension of the domain of the posterior, $\text{Cov}(\boldsymbol{\theta}_0, \boldsymbol{\theta}_1, ..., \boldsymbol{\theta}_{n-1})$ is the covariance matrix computed from the previous states of the chain, λ is an arbitrarily small positive constant and $\mathbf{I}_d$ is the d–dimensional identity matrix.

Therefore, given a current state $\boldsymbol{\theta}_n$ of the Markov Chain, a candidate $\boldsymbol{\theta}_1^*$ is generated, from an auxiliary probability density function $q_1(\boldsymbol{\theta}_1^*|\boldsymbol{\theta}_n)$, and it is accepted with probability α_1 given as follows

$$\alpha_1(\boldsymbol{\theta}_n, \boldsymbol{\theta}_1^*) = \min\left\{1, \frac{\pi(\boldsymbol{\theta}_1^*|\mathbf{z}_E)\, q_1(\boldsymbol{\theta}_n|\boldsymbol{\theta}_1^*)}{\pi(\boldsymbol{\theta}_n|\mathbf{z}_E)\, q_1(\boldsymbol{\theta}_1^*|\boldsymbol{\theta}_n)}\right\} \tag{26}$$

where $\pi(\boldsymbol{\theta}|\mathbf{z}_E)$ is the target probability density function.

Upon acceptance, the candidate is the new state of the chain, $\boldsymbol{\theta}_{n+1} = \boldsymbol{\theta}_1^*$. Otherwise, upon rejection of the candidate $\boldsymbol{\theta}_1^*$, instead of retaining the current state, as it is done in the standard Metropolis-Hastings algorithm, a second candidate $\boldsymbol{\theta}_2^*$ is proposed from the auxiliary probability density function $q_2(\boldsymbol{\theta}_2^*|\boldsymbol{\theta}_n, \boldsymbol{\theta}_1^*)$. Then, the second candidate is accepted with probability α_2 given as

$$\alpha_2(\boldsymbol{\theta}_n, \boldsymbol{\theta}_1^*, \boldsymbol{\theta}_2^*) = \min\left\{1, \frac{\pi(\boldsymbol{\theta}_2^*|\mathbf{z}_E)\, q_1(\boldsymbol{\theta}_1^*|\boldsymbol{\theta}_2^*)\, q_2(\boldsymbol{\theta}_n|\boldsymbol{\theta}_2^*, \boldsymbol{\theta}_1^*)\left[1 - \alpha_1(\boldsymbol{\theta}_2^*, \boldsymbol{\theta}_1^*)\right]}{\pi(\boldsymbol{\theta}_n|\mathbf{z}_E)\, q_1(\boldsymbol{\theta}_1^*|\boldsymbol{\theta}_n)\, q_2(\boldsymbol{\theta}_2^*|\boldsymbol{\theta}_n, \boldsymbol{\theta}_1^*)\left[1 - \alpha_1(\boldsymbol{\theta}_n, \boldsymbol{\theta}_1^*)\right]}\right\} \tag{27}$$

In the DR strategy, within a step of the Markov Chain, the process of generating new candidates from the current state and previously rejected candidates, may be performed for a fixed or random number of stages. Therefore, at the i-th stage of the DR strategy, the candidate $\boldsymbol{\theta}_i^*$ is accepted with probability

$$\begin{aligned} &\alpha_i(\boldsymbol{\theta}_n, \boldsymbol{\theta}_1^*, \dots, \boldsymbol{\theta}_i^*) = \\ &\min\left\{1, \frac{\pi(\boldsymbol{\theta}_i^*|\mathbf{z}_E) q_1(\boldsymbol{\theta}_{i-1}^*|\boldsymbol{\theta}_i^*)\, q_2(\boldsymbol{\theta}_{i-2}^*|\boldsymbol{\theta}_i^*, \boldsymbol{\theta}_{i-1}^*) \dots q_i(\boldsymbol{\theta}_n|\boldsymbol{\theta}_i^*, \boldsymbol{\theta}_{i-1}^*, \dots)}{\pi(\boldsymbol{\theta}_n|\mathbf{z}_E) q_1(\boldsymbol{\theta}_1^*|\boldsymbol{\theta}_n)\, q_2(\boldsymbol{\theta}_2^*|\boldsymbol{\theta}_n, \boldsymbol{\theta}_1^*) \dots q_i(\boldsymbol{\theta}_i^*|\boldsymbol{\theta}_n, \boldsymbol{\theta}_1^*, \dots)}\right. \\ &\left.\frac{[1 - \alpha_1(\boldsymbol{\theta}_i^*, \boldsymbol{\theta}_{i-1}^*)][1 - \alpha_2(\boldsymbol{\theta}_i^*, \boldsymbol{\theta}_{i-1}^*, \boldsymbol{\theta}_{i-2}^*)] \dots [1 - \alpha_{i-1}(\boldsymbol{\theta}_i^*, \dots, \boldsymbol{\theta}_1^*)]}{[1 - \alpha_1(\boldsymbol{\theta}_n, \boldsymbol{\theta}_1^*)][1 - \alpha_2(\boldsymbol{\theta}_n, \boldsymbol{\theta}_1^*, \boldsymbol{\theta}_2^*)] \dots [1 - \alpha_{i-1}(\boldsymbol{\theta}_n, \boldsymbol{\theta}_1^*, \dots, \boldsymbol{\theta}_{i-1}^*)]}\right\} \end{aligned} \tag{28}$$

In the higher stages of the DR algorithm, the auxiliary probability density functions are also multivariate Gaussians centred at the current state of the chain and with covariance matrices given by scaled versions of the covariance matrix of the fist stage, that is, $q_i \sim N(\theta_n, \gamma_i \mathbf{C}_n^1)$ where γ_i is a *shrinkage factor*.

The procedure previously describe is repeated until a Markov chain is generated with an arbitrary number N_s of states, in the form $\{\theta_1, \theta_2, ..., \theta_{N_s}\}$. In practice, the initial states of the generated chain, named *burn-in* states, are not a representative sample of the target posterior probability density function and, therefore, are discarded for further analyses. After discarding the N_b burn-in states, the resulting chain $\{\theta_{N_b+1}, \theta_{N_b+2}, ..., \theta_{N_s}\}$ is supposed to reach stationarity and, therefore, is used for inference of the target posterior probability density function.

NUMERICAL RESULTS

This section is concerned with the numerical assessment of the proposed Bayesian damage identification approach based on a RSM of the reduced flexibility matrix of the structure. Damage identification problems in a rectangular simply supported steel plate are considered. The nominal geometric and material properties of the plate are presented in Table I.

Table I. Nominal geometric and material properties of the plate.

Length	0.6 m
Width	0.6 m
Thickness (h_0)	0.002 m
Mass density	7851 kg/m^3
Young modulus	210 GPa
Poisson ratio	0.33

The flexibility matrix of the structure was derived considering the Kirchhoff plate theory and a spatial discretization of the plate into 6×6 hermitian rectangular finite elements with four corner nodes. The displacement and the cohesion fields were approximated by the same finite element mesh and, therefore, in each node of a finite element, one has three DOF – one translational, one rotational about x and one rotational about y – and one nodal cohesion parameter. Hence, the present FEM of the plate has $n_p = 49$ nodal cohesion parameters for the description of its structural integrity.

Without loss of generality and for the sake of simplicity, in the numerical analyses that follow, it is assumed that structural damages only alter the thickness of the plate. Hence, the Young's modulus and the Poisson's ratio are assumed as known and uniform within the plate, that is $E(x, y) = E_0$ and $\nu(x, y) = \nu_0$. Therefore, considering Eqs. (1) to (3), the cohesion filed may be written as a function only of the relative thickness of the plate, viz.

$$\beta(x, y) = \left(\frac{h(x, y)}{h_0} \right)^3 . \tag{29}$$

Due to the considered bilinear shape functions used to interpolate the cohesion field, a damage scenario prescribed by only one nodal cohesion parameter different from unity and away from the boundary of the plate has a pyramid shape, and it encompass four finite elements. On the other hand, a damage prescribed by only one nodal cohesion parameter different from unity at the boundary of the plate encompass only two finite elements and has, therefore, a half pyramid shape.

Due to the simply supported boundary condition, the responses of the plate present very low sensitivities with respect to the nodal cohesion parameters at its edges. Therefore, these parameters were not estimated in the damage identification problems that follow, yielding a vector of uncertain parameters $\boldsymbol{\theta}$ with 25 nodal parameters.

A RSM of the reduced flexibility matrix, built on the second order polynomial in Eq. (19), was used in the Bayesian inverse problems of damage identification present in what follows. The nodal cohesion parameters and the corresponding coded parameters, according to Eq. (15), used to generate the training data of the RSM are presented in Table II. In order to give some insight about the damage severities, the corresponding relative thicknesses of the plate, where the damages are more severe, are also presented. For the synthesis of the RSM it was assumed that the damage identification approach is capable of identifying structural damages in an early stage and that the structural damages are localized events. Based on these assumptions, in the present work, it was considered that the damage state of the structure may be described by up to three nodal cohesion parameters different from unity. Hence, considering the values presented in Table II, the training data of the RSM were obtained by combinations of 25 nodal cohesion parameters taken up to three at a time ($C_1^{25} + C_2^{25} + C_3^{25}$) added with $2n_p$ axial points, one point corresponding to the undamaged state (all cohesion parameters equal to the unity) and one central point (all cohesion parameters equal to 0.756). In the combination C_r^{25}, r nodal cohesion parameters were set at the value 0.512 and the others were set at 1. A total of 2677 training data were used to train the RSM of the reduced flexibility matrix. It is worth emphasizing that a Centre Composite Design would require a total of 33554483 training data.

Table II. Nodal cohesion parameters and coded parameters adopted in the synthesis of the RSM.

Cohesion Parameter (β_d)	Relative Thickness (h_d/h_0)	Coded Parameter (x)
0.189	0.57	−2.325
0.512	0.80	−1
0.756	0.91	0
1.000	1.00	+1
1.323	1.10	+2.325

The damage scenarios considered in the numerical simulations that follow are presented in Table III. The damage position means the location of the vertex of the pyramid shape notch and β_d and h_d/h_0 are, respectively, the nodal cohesion parameter and the relative thickness of the plate at this position.

Table III. Damage scenarios.

Scenario	Damage Position (x_d, y_d) (m)	β_d	h_d/h_0
A	(0.3, 0.3)	0.512	0.8
B	(0.3, 0.2);(0.2, 0.5)	0.512; 0.729	0.8; 0.9
C	(0.2, 0.1);(0.4, 0.5)	0.729; 0.729	0.9; 0.9

The adopted finite element mesh, the measured transversal DOF used in the damage identification process, and the considered damage scenarios are illustrated in Fig. 1.

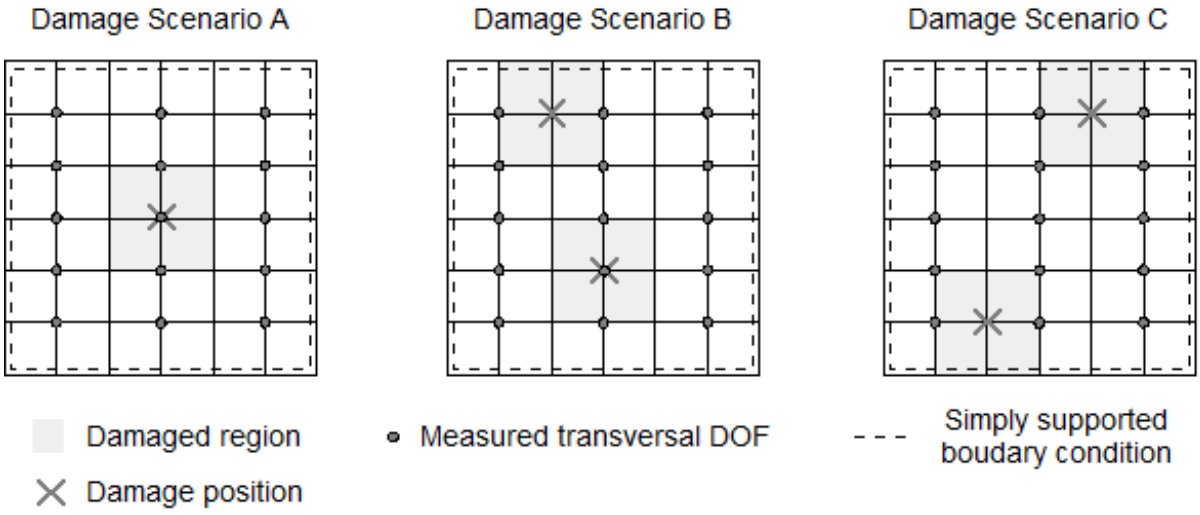

Figure 1. Finite element mesh, damaged scenarios and sensor placement.

For the computation of the synthetic experimental flexibility matrix, it was considered that only the first six modes of vibration were measured and that the mode shapes are composed of the vertical displacements at the measurement points pinpointed in Fig. 1. Besides, with the aim at simulating both the corrupting effects of noise in the measured data and the errors associated with the modal extraction methods, the reduced flexibility matrix of the supposed damaged structure is computed considering the following synthetic experimental mode shapes.

$$\boldsymbol{\phi}_{iE} = \boldsymbol{\phi}^0_{iE} + \mathbf{r}, \qquad i = 1, 2, \ldots n_E, \tag{30}$$

where $\boldsymbol{\phi}^0_{iE}$ is the i-th synthetic experimental mode shape without noise, $\mathbf{r}$ is a vector whose components are independent and normally distributed random numbers, with zero mean and variance σ_r^2, and n_E is the number of mode shapes retained in the synthetic modal test (Ramos et al. 2010, Jaishi & Ren 2006, Tomaszewska 2010). In the present work, one has $n_E = 10$ and three different noise levels, corresponding to $\sigma_r = 0.005$, 0.01 and 0.015. Four damage identification cases were considered, as presented in Table IV.

Since the damage identification problem was formulated based on the generalized response vector $\hat{\mathbf{z}}$, which is composed of elements of the reduced flexibility matrix provided by the RSM,

Table IV. Damage identification cases: Damage scenarios and noise levels.

Case	Damage Scenario	σ_r
A1	A	0.005
A2	A	0.015
B1	B	0.010
C1	C	0.005

the measurement error vector $\boldsymbol{\epsilon}$, in Eq. (23), has correlated components. Hence, an estimate of its covariance matrix $\mathbf{V}$, used in the likelihood function defined in Eq. (24), was computed considering 1000 realizations of the synthetic experimental response $\mathbf{z}_E$.

As prior information, it was assumed that structural damages are localized events, which means that damaged regions occupy relatively small portions of the structure domain. Hence, most of the uncertain parameters are within undamaged regions, where the cohesion field has a unit value. Besides, it was also considered that structural damages can be identified in early stages. This information was translated in the marginal prior probability density function given by

$$p(\theta_i) = \begin{cases} 0, & \text{if} \quad \theta_i < 0.4 \\ c\, N\left(1, 0.05^2\right), & \text{if} \quad 0.4 \leq \theta_i \leq 1.04 \\ 0, & \text{if} \quad \theta_i > 1.04 \end{cases} \tag{31}$$

where $N\left(1, 0.05^2\right)$ is a Gaussian distribution with unity mean and standard deviation of 0.05, and c is the normalizing constant that ensures that the marginal prior probability density function integrates to 1. According to Eq. (31), the most probable value of a uncertain parameter (a nodal cohesion parameter, in the present case) is one.

In the following numerical results, the DRAM algorithm was used draw samples from the posterior probability density function of the uncertain parameters. In each damage identification case, Markov chains with 50,000 states were generated, where the first 30,000 were considered burn-in states. The initial value of the uncertain parameters was adopted as one, which means that a undamaged plate was considered at the beginning of the Bayesian damage identification process.

A DRAM algorithm with three stages and a multivariate Gaussian auxiliary probability density function was considered. According to Eq. (25), during the non-adaptation period of the algorithm, $n \leq 5000$, the covariance matrix of the auxiliary probability density function, in the first stage, was adopted as $\mathbf{C}_0 = \text{diag}(\sigma_1^2, \ldots, \sigma_{25}^2)$, with $\sigma_i = 0.005$ for $i = 1, \ldots, 25$. After this period, the covariance matrix of the auxiliary density function of the first stage was adapted in each iteration of the algorithm considering previous states of the chain. However, for the adaptation of the covariance matrix the first 500 states of the chain were not taken into account. At the second and third stages of the DRAM algorithm, which represent delayed rejection steps, the covariance matrix of the auxiliary density functions was obtained by scaling the covariance matrix in the first stage by a shrinkage factor $\gamma_i = 0.01$ for $i = 2, 3$.

Figures 2 and 3 present the damage identification results for Case A1. The estimated cohesion field presented in Fig. 2a shows that the damage position in the present case was accurately identified. Figure 2b presents the relative frequency errors obtained for the initial model, which considers an undamaged structure, and for the updated model, corresponding to the estimated cohesion field. The relative frequency errors were computed as

$$\omega_{\text{error}} = \frac{|\omega_{iE} - \omega_i|}{\omega_{iE}}, \tag{32}$$

where ω_{iE} is the i-th experimental undamped natural frequency and ω_i is the corresponding one predicted by the model.

As can be clearly observed in Fig. 2b, the relative frequency errors provided by the updated model are considerably lower, demonstrating a good adherence of the predicted responses to the experimental data.

Figure 3a presents the Markov Chains of all 25 unknown parameters, which visually converged to their equilibrium after approximately 10,000 states, as pinpointed in the autocorrelation function (ACF) presented in Fig. 3b for the nodal cohesion parameter associated to the damage position. This same parameter clearly converged to the neighborhood of the exact value β_d, which was used in the simulation of the experimental data. This result demonstrate that the damage intensity was also accurately estimated. The histogram of the nodal cohesion parameter associated to the damage position is depicted in Fig. 3c, showing that a relatively small dispersion was achieved, encompassing the exact value.

The estimated cohesion field and the corresponding relative frequency errors for the damage identification problem of Case A2 are presented in Figs. 4a and 4b, respectively. It must be highlighted that Cases A1 and A2 differ from each other just in the level of noise in the synthetic experimental data (see Table IV). From Fig. 4a, one may observe that the actual damage position was again accurately pinpointed, despite the presence of a higher level of noise in the synthetic experimental data. The higher level of noise in this case also yield the identification of a false damaged region, with a relatively low intensity, as can be observed in Fig. 4a. The relative frequency errors depicted in Fig. 4b show that the natural frequencies predicted by the updated model are closer to the corresponding experimental ones than those predicted by the initial model.

The Markov Chains of all uncertain parameters are depicted in Fig. 5a for Case A2. As can be clearly seen in Fig. 5a, once again the states of just one uncertain parameter converged to the neighborhood of the exact value β_d. Besides, as expected, due to the higher level of noise in the experimental data, greater dispersions are observed in the states of the chains. The ACF and the histogram of the nodal cohesion parameter associated to the damage position are depicted in Figs. 5b and 5c, respectively. Figure 5b shows that the Markov Chain of this parameter converged to its equilibrium after approximately 10,000 states. Comparing Figs. 3c and 5c, one may clearly note the greater dispersion of the states in the damage identification of Case A2 due to the higher level of noise.

Figures 6 and 7 present the damage identification results for Case B1, which considers two damaged regions, with different damage intensities and apart from each other, and a moderate level of noise in the synthetic experimental data. The estimated cohesion field is presented in Fig. 6a, which shows that the location of the two actual damaged regions were accurately pinpointed

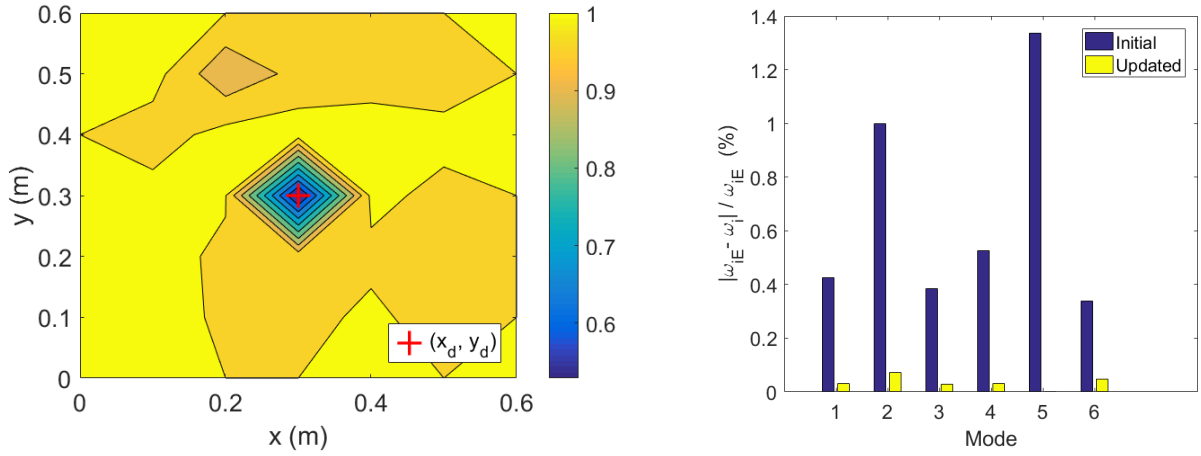

(a) (b)

Figure 2. (a) Estimated cohesion field and (b) Frequency relative errors for Case A1.

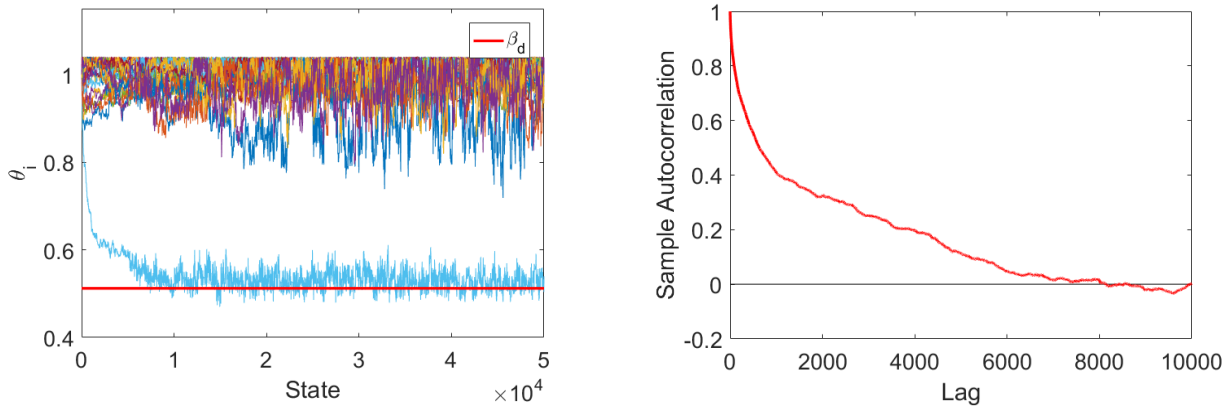

(a) (b)

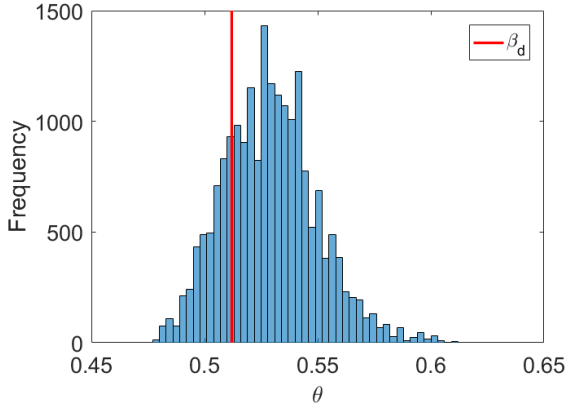

(c)

Figure 3. (a) Markov chains of the uncertain parameters, (b) ACF of the nodal cohesion parameter associated with the damage and (c) its histogram for Case A1.

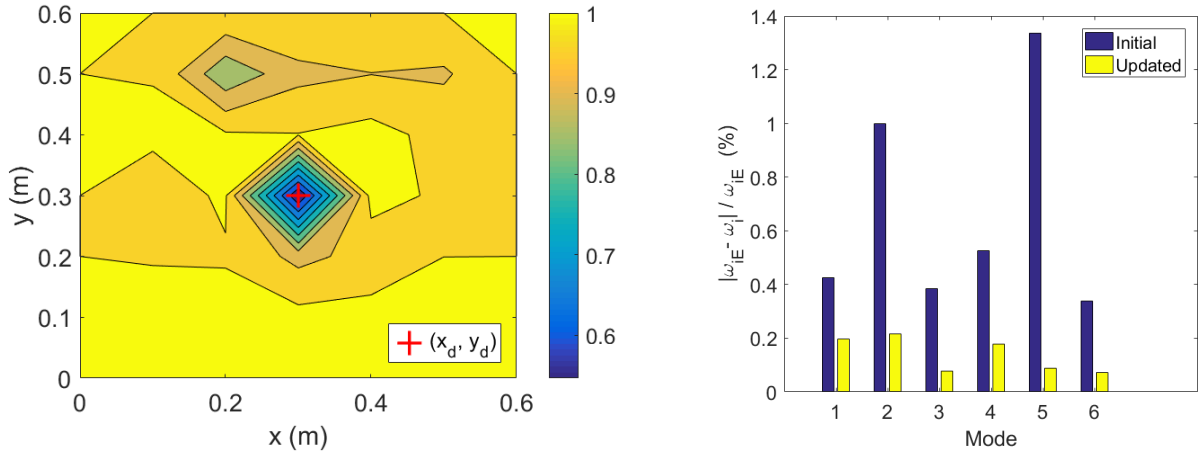

(a) (b)

Figure 4. (a) Estimated cohesion field and (b) Frequency relative errors for Case A2.

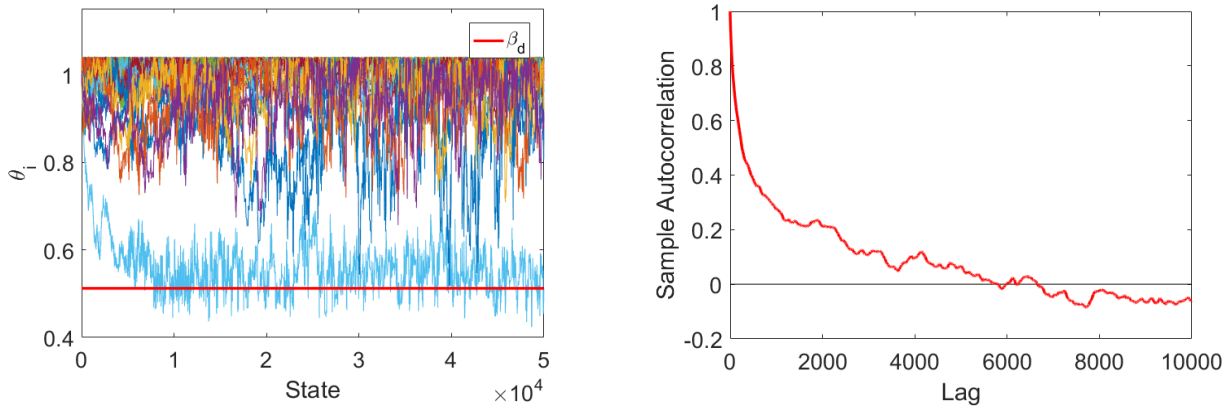

(a) (b)

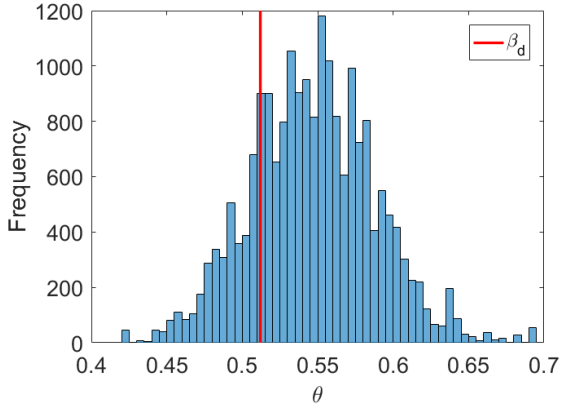

(c)

Figure 5. (a) Markov chains of the uncertain parameters, (b) ACF of the nodal cohesion parameter associated with the damage position and (c) its histogram for Case A2.

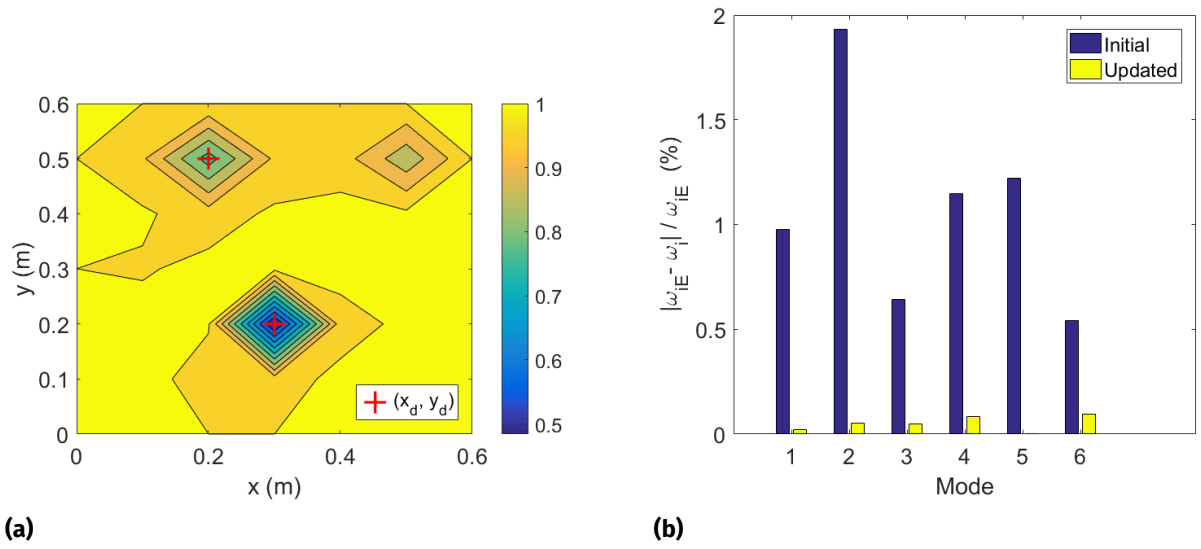

Figure 6. (a) Estimated cohesion field and (b) Frequency relative errors for Case B1.

by the proposed approach. Although a false damaged region was also pinpointed in this case, the corresponding damage intensity is relatively slow. Figure 6b shows that the updated model can accurately predict the natural frequencies of the damaged structure, which indicates that the estimated damage profile, depicted in Fig. 6a, can be considered satisfactory.

The ACFs and the histograms of the nodal cohesion parameters associated with the two damage positions are depicted in Fig. 7. The ACFs depicted in Figs. 7b and 7c indicate that the Markov Chain of one uncertain parameter (the nodal cohesion parameter associated with the damage position x_d = 0.3 m and y_d = 0.2 m) converged to its equilibrium more quickly than the other. This can be explained by the fact that the damage located near the edge of the plate, in addition to having a lower intensity, is within a region where the structural response presents a lower sensitivity to the presence of damages, in the case of a simply supported plate. The dispersion of the uncertain parameters, associated with the damage positions, about their exact values (β_d) can be observed from the histograms in Figs. 7d and 7e.

Finally, the damage identification results for Case C1 are presented in Figs. 8 and 9. In this case, one has two damaged regions with low intensities and apart from each other. Besides, a low level of noise (σ_r = 0.005) was considered in the synthetic experimental data. Figure 8 shows that the damage locations were accurately identified and that the natural frequencies predicted by the updated model are closer to the corresponding experimental ones than those predicted by the initial model.

Comparing the ACFs presented in Figs. 9b and 9c, it can be observed that the Markov Chain of the uncertain parameter associated with the the first damage position (x_d = 0.2m, y_d = 0.1m) converged faster than the chain of the associated parameter of the second damage position (x_d = 0.4m, y_d = 0.5m). Furthermore, from Figs. 9d and 9e, it can be seen that the histogram of the uncertain parameter associated with the first damage presents a sample mean closer to the exact value β_d and with a smaller dispersion around it.

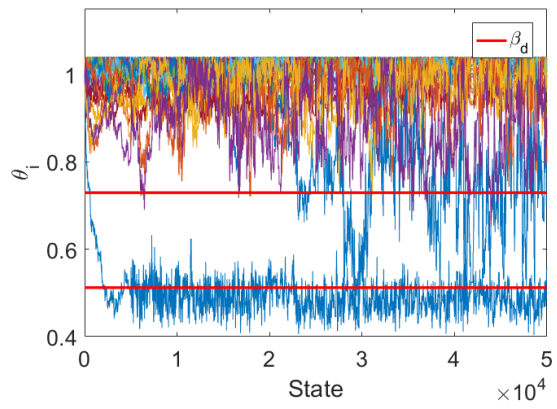

(a)

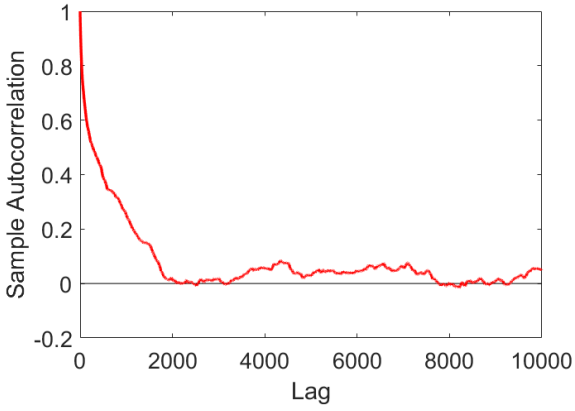

(b)

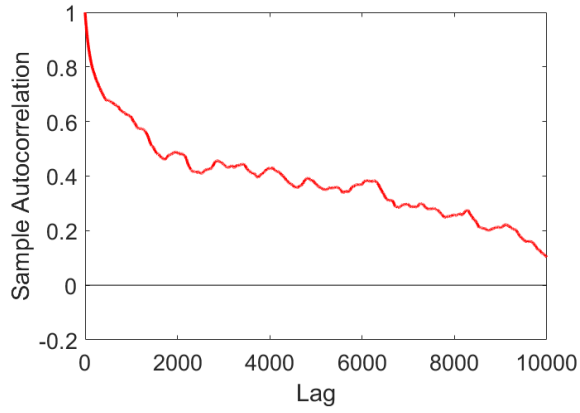

(c)

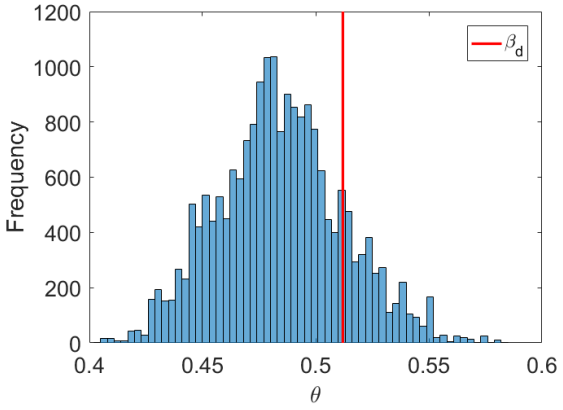

(d)

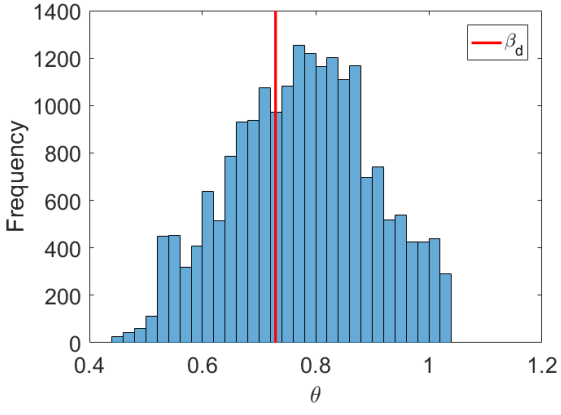

(e)

Figure 7. (a) Markov chains of the uncertain parameters, (b)-(c) ACFs of the nodal cohesion parameters associated with the damage positions and (d)-(e) their histograms for Case B1.

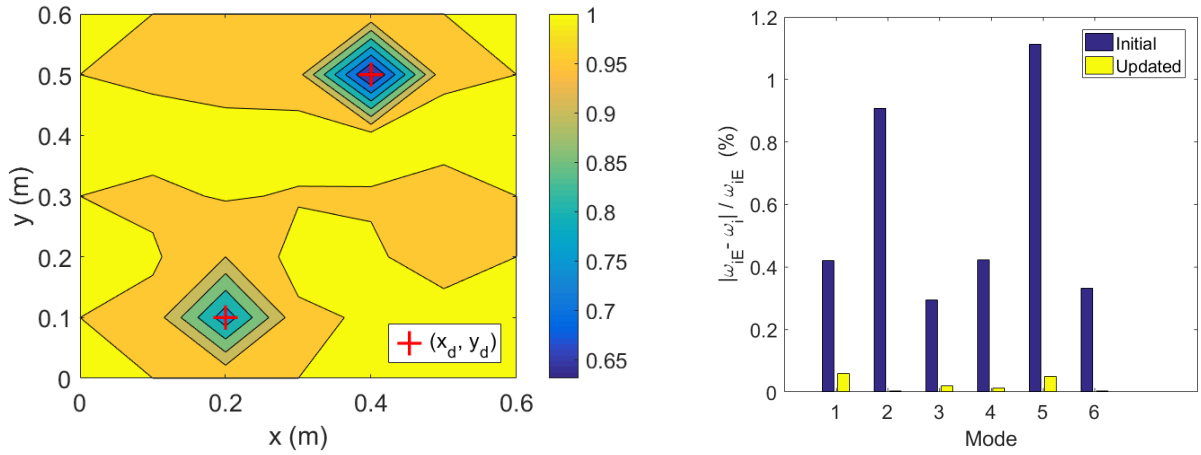

(a) **(b)**

Figure 8. (a) Estimated cohesion field and (b) Frequency relative errors for Case C1.

Table V presents the computational costs of the proposed damage identification method in solving the inverse problems presented above. For comparison purposes, the computational costs obtained when the reduced flexibility matrix directly obtained from the FEM of the structure is used in the inverse problems are also presented. The computational costs were obtained in a computer with a 2.1 Ghz Intel® Core™ i7 processor with 6 GB of RAM.

Table V. Execution time (min).

Approach	Case			
	A1	A2	B1	C1
RSM	10.66	11.30	10.24	11.81
FEM	44.51	43.49	45.87	45.03

CONCLUSIONS

The present work presented a Bayesian damage identification approach built on a RSM of the reduced flexibility matrix of the structure. The RSM was fitted using training data obtained by combinations of a relatively small number of nodal cohesion parameters, which required a considerably lower number of numerical simulations than would be used by the classical CCD method. The inverse damage identification problem was formulated within the Bayesian framework and the DRAM method was used to sample the joint posterior probability density function of the uncertain parameters used to describe the damage state of the structure. Numerical results showed that the proposed damage identification approach succeeded in the identification of different damage profiles in a simply supported plate. The results also showed that the proposed approach yielded a reduction of up to almost 78% in the

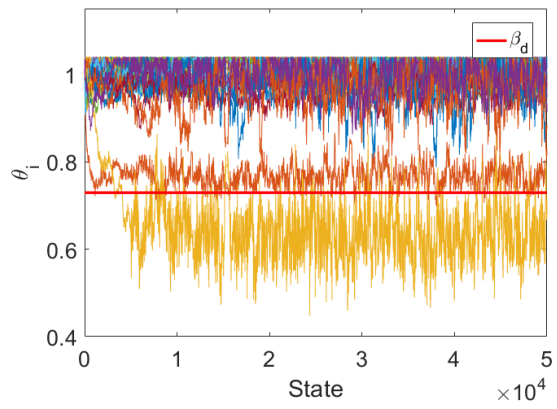

(a)

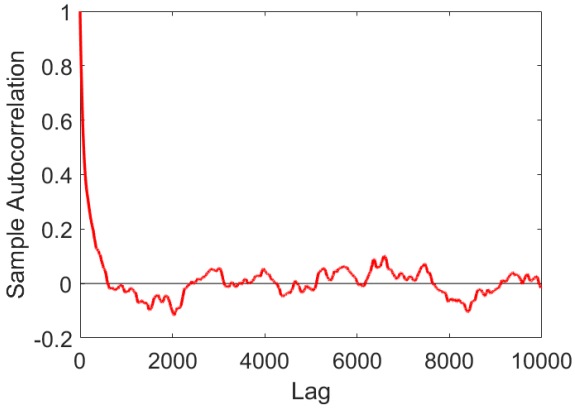

(b)

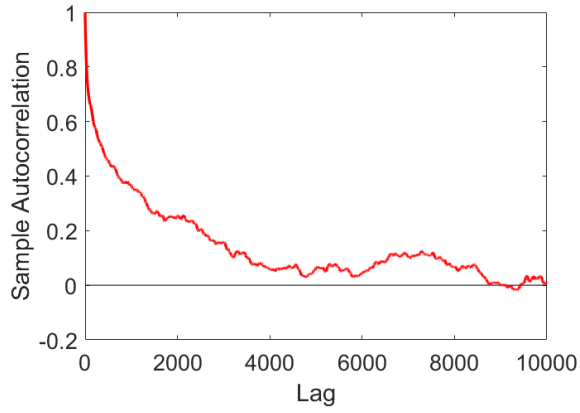

(c)

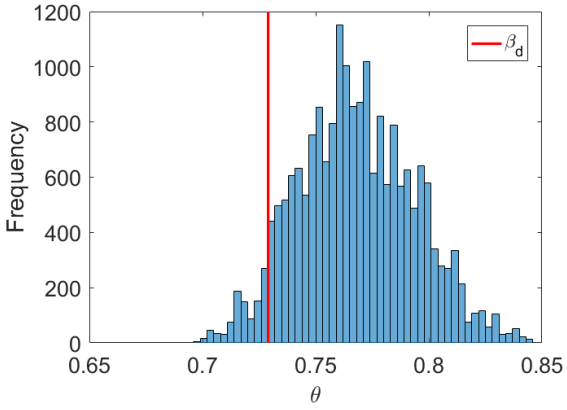

(d)

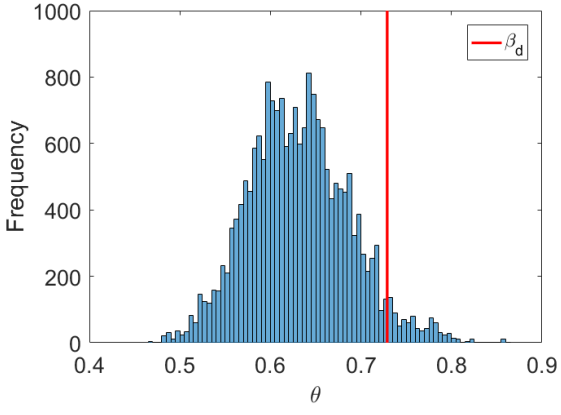

(e)

Figure 9. (a) Markov chains of the uncertain parameters, (b)-(c) ACFs of the nodal cohesion parameters associated with the damage positions and (d)-(e) their histograms for Case C1.

computation cost that would be required if the flexibility matrix directly obtained from a FEM of the structure had been used in the inverse process.

Acknowledgments

The authors acknowledge the financial support provided by the Fundação Carlos Chagas Filho de Amparo à Pesquisa do Estado do Rio de Janeiro (FAPERJ) and the Conselho Nacional de Desenvolvimento Científico e Tecnológico (CNPq). This study was also financed in part by the Coordenação de Aperfeiçoamento de Pessoal de Nível Superior – Brazil (CAPES) – Finance Code 001.

REFERENCES

ALVIN K, ROBERTSON A, REICH G & PARK K. 2003. Structural system identification: from reality to models. Comput Struct 81(12): 1149-1176.

BECK JL & AU SK. 2002. Bayesian updating of structural models and reliability using Markov Chain Monte Carlo Simulation. J Eng Mech 128(4): 380-391.

CHEN DM, XU YF & ZHU WD. 2018. Identification of damage in plates using full-field measurement with a continuously scanning laser Doppler vibrometer system. J Sound Vib 422: 542-567.

CHEUNG SH & BECK JL. 2009. Bayesian Model Updating Using Hybrid Monte Carlo Simulation with Application to Structural Dynamic Models with Many Uncertain Parameters. J Eng Mech 135(4): 243-255.

CHING J & CHEN YC. 2007. Transitional Markov Chain Monte Carlo Method for Bayesian Model Updating, Model Class Selection, and Model Averaging. J Eng Mech 133(7): 816-832.

CHING J & WANG JS. 2016. Application of the transitional Markov chain Monte Carlo algorithm to probabilistic site characterization. Eng Geol 203: 151-167.

DESSI D & CAMERLENGO G. 2015. Damage identification techniques via modal curvature analysis: Overview and comparison. Mech Sys Sign Process 52-53: 181-205.

EREIZ S, DUVNJAK I & JIMÉNEZ-ALONSO JF. 2022. Review of finite element model updating methods for structural applications. Structures 41: 684-723.

FANG SE & PERERA R. 2011. Damage identification by response surface based model updating using D-optimal design. Mech Syst Signal Process 25: 717-733.

FU YZ, LU ZR & LIU JK. 2013. Damage identification in plates using finite element model updating in time domain. J Sound Vib 232: 7018-7032.

GAMERMAN D & LOPES HF. 2006. Markov Chain Monte Carlo: stochastic simulation for Bayesian inference. Chapman & Hall/CRC.

GARDNER P, ROGERS T, LORD C & BARTHORPE R. 2021. Learning model discrepancy: A Gaussian process and sampling-based approach. Mech Sys Sign Process 152: 107381.

GHIASI R, GHASEMI MR & NOORI M. 2018. Comparative studies of metamodeling and AI-Based techniques in damage detection of structures. Adv Eng Softw 125: 101-112.

HAARIO H, LAINE M, MIRA A & SAKSMAN E. 2006. DRAM: efficient adaptive MCMC. Stat Comput 16(4): 339-354.

HAARIO H, SAKSMAN E & TAMMINEN J. 2001. An adaptive Metropolis algorithm. Brenoulli 7(2): 223.

HOU R & XIA Y. 2021. Review on the new development of vibration-based damage identification for civil engineering structures: 2010-2019. J Sound Vib 491: 115741.

HUANG T & SCHRÖDER KU. 2021. A Bayesian probabilistic approach for damage identification in plate structures using responses at vibration nodes. Mech Sys Sign Process 146: 106998.

HUANG Y, SHAO C, WU B, BECK JL & LI H. 2018. State-of-the-art review on Bayesian inference in structural system identification and damage assessment. Adv Struct Eng 22: 1329-1351.

JAISHI B & REN W. 2006. Damage detection by finite element model updating using modal flexibility residual. J Sound Vib 290: 369-387.

JIN SS & JUNG HJ. 2016. Sequential surrogate modeling for efficient finite element model updating. Comput Struct 168: 30-45.

KAIPIO J & SOMERSALO E. 2004. Statistical and Computational Inverse Problems. New York: Springer.

KIRSCH A. 1996. An Introduction to the Mathematical Theory of Inverse Problems. Berlin: Springer.

KONG X, CAI CS & HU J. 2017. The State-of-the-Art on Framework of Vibration-Based Structural Damage Identification for Decision Making. Applied Sciences 7(5): 495.

LEISSA AW & QATU MS. 2011. Vibration of Continuous Systems. New York: McGraw-Hill.

LI M, JIA D, WU Z, QIU S & HE W. 2022. Structural damage identification using strain mode differences by the iFEM based

on the convolutional neural network (CNN). Mech Sys Sign Process 165: 108289.

LIU JS & CHEN R. 1998. Sequential Monte Carlo Methods for Dynamic Systems. J Am Stat Assoc 93(443): 1032-1044.

LYE A, CICIRELLO A & PATELLI E. 2021. Sampling methods for solving Bayesian model updating problems: A tutorial. Mech Syst Signal Pr 159: 107760.

MARTINO L. 2018. A review of multiple try MCMC algorithms for signal processing. Dig Sig Process 75: 134-152.

MARTINO L & READ J. 2013. On the flexibility of the design of multiple try Metropolis schemes. Computation Stat 28: 2797-2823.

MARWALA T, BOULKAIBET I & ADHIKARI S. 2016. Probabilistic Finite Element Model Updating Using Bayesian Statistics: Applications to Aeronautical and Mechanical Engineering. New Jersey: J Wiley & Sons.

MEIROVITCH L. 1986. Elements of Vibration Analysis. Singapore: McGraw-Hill.

MIRA A. 2001. On Metropolis-Hastings algorithms with delayed rejection. Metron 59(3-4): 231-241.

MONTGOMERY DC. 2006. Design and analysis of experiments. New York: J Wiley & Sons.

MONTGOMERY DC & RUNGER GC. 2014. Applied Statistics and Probability for Engineers. New York: J Wiley & Sons.

MYERS RH, MONTGOMERY DC & A-COOK CM. 2009. Response Surface Methodology: Process and Product Optimization Using Designed Experiments. New Jersey: J Wiley & Sons.

NEAL RM. 2011. MCMC using Hamiltonian dynamics. In: Brooks S, Gelman A, Jones G & Meng XL (Eds), Handbook of Markov Chain Monte Carlo, Chapman and Hall/CRC.

NI P, LI J, HAO H, HAN Q & DU X. 2021. Probabilistic model updating via variational Bayesian inference and adaptive Gaussian process modeling. Comput Method App Mech Eng 383: 113915.

PRAKASH G & NARASIMHAN S. 2018. Bayesian Two-Phase Gamma Process Model for Damage Detection and Prognosis. J Eng Mech 144(2): 04017158.

RAMANCHA MK, VEGA MA, CONTE JP, TODD MD & HU Z. 2022. Bayesian model updating with finite element vs surrogate models: Application to a miter gate structural system. Eng Struct 272: 114901.

RAMOS LF, ROECK GD, CO PBL & CAMPOS-COSTA A. 2010. Damage identification on arched masonry structures using ambient and random impact vibrations. Eng Struct 32: 146-162.

RANDALL RB. 2021. Vibration-based condition monitoring: industrial, automotive and aerospace applications. New Jersey: J Wiley & Sons.

REDDY JN. 1984. An Introduction to the finite Element Method. New York: McGraw-Hill.

RENS KL, WIPF TJ & KLAIBER FW. 1997. Review of Nondestructive Evaluation Techniques of Civil Infrastructure. J Perform Contr Facil 11(4): 152-160.

ROCCHETTA R, BROGGI M, HUCHET Q & PATELLI E. 2018. On-line Bayesian model updating for structural health monitoring. Mech Syst Signal Pr 103: 174-195.

SBARUFATTI C, MANES A & GIGLIO M. 2013. Performance optimization of a diagnostic system based upon a simulated strain field for fatigue damage characterization. Mech Sys Sign Process 40(2): 667-690.

SILVA GLS, CASTELLO DA, BORGES L & KAIPIO JP. 2020. Damage identification in plates under uncertain boundary conditions. Mech Sys Sign Process 144: 106884.

SILVA GLS, CASTELLO DA & KAIPIO JP. 2021. Damage identification under uncertain mass density distributions. Comput Method App Mech Eng 376: 113672.

SIMOEN E, ROECK GD & LOMBAERT G. 2015. Dealing with uncertainty in model updating for damage assessment: A review. Mech Sys Sign Process 56-57: 123-149.

STUTZ LT, RANGEL ICSS, RANGEL LS, CORRÊA RAP & KNUPP DC. 2018. Structural damage identification built on a response surface model and the flexibility matrix. J Sound Vib 434: 284-297.

TALAEI S, BEITOLLAHI A, MOSHIRABADI S & FALLAHIAN M. 2018. Vibration-based Structural Damage Detection Using Twin Gaussian Process (TGP). Structures 16: 10-19.

TOMASZEWSKA A. 2010. Influence of statistical errors on damage detection based on structural flexibility and mode shape curvature. Comput Struct 88: 154-164.

UMAR S, BAKHARY N & ABIDIN ARZ. 2018. Response surface methodology for damage detection using frequency and mode shape. Measurement 115: 258-268.

WARNER JE, HOCHHALTER JD, LESER WP, LESER PE & NEWMAN JA. 2016. A computationally-efficient inverse approach to probabilistic strain-based damage diagnosis. In: Annual Conference of the PHM Society. Vol. 8.

YUEN KV & KUOK S. 2011. Bayesian Methods for Updating Dynamic Models. Appl Mech Rev 64(1): 010802.

How to cite
STUTZ LT, KNUPP DC, ABREU LAS, RANGEL ICSS, RANGEL LS & CORRÊA RAP. 2024. Response Surface Model of the Reduced Flexibility Matrix for Bayesian Damage Identification. An Acad Bras Cienc 96: e20230953. DOI 10.1590/0001-3765202420230953.

Manuscript received on August 28, 2023;
accepted for publication on March 3, 2024

LEONARDO T. STUTZ[1]
https://orcid.org/0000-0003-3005-765X

DIEGO C. KNUPP[1]
https://orcid.org/0000-0001-9534-5623

LUIZ ALBERTO S. ABREU[1]
https://orcid.org/0000-0002-7634-7014

ISABELA CRISTINA S.S. RANGEL[2]
https://orcid.org/0009-0004-2192-2511

LUCIANO S. RANGEL[2]
https://orcid.org/0009-0006-3631-3780

ROSILENE A.P. CORRÊA[3]
https://orcid.org/0009-0002-4523-5025

[1]Pós-Graduação em Modelagem Computacional, Universidade Estadual do Rio de Janeiro, Instituto Politécnico, Rua Hormindo Silva, 25, 28625-570 Nova Friburgo, RJ, Brazil
[2]Faculdade Municipal Miguel Ângelo da Silva Santos, Rua Aloísio da Silva Gomes, 50, 27930-560 Macaé, RJ, Brazil
[3]Universidade Federal Fluminense, Instituto do Noroeste Fluminense de Educação Superior, Estrada João Jasbick, s/n, 28470-000 Santo Antônio de Pádua, RJ, Brazil

Correspondence to: **Leonardo Tavares Stutz**
E-mail: ltstutz@iprj.uerj.br

Author contributions

Conceptualization: LTS, DCK and ICSSR; methodology: LTS, DCK, ICSSR, LSR, RAPC and LASA; data curation: LTS, DCK and ICSSR; validation: LTS, DCK and ICSSR; writing–original draft preparation: LTS, DCK, ICSSR and LSR; writing–review and editing: LTS, DCK, ICSSR, LSR, RAPC and LASA.

CC BY